ACS OMEGA

Article

http://pubs.acs.org/journal/acsodf

Metal–Organic Framework/Graphene Quantum Dot Nanoparticles Used for Synergistic Chemo- and Photothermal Therapy

Zhengfang Tian,[†,∥] Xianxian Yao,[‡,∥] Kexin Ma,[‡] Xingxing Niu,[‡] Julia Grothe,[§] Qingni Xu,[†] Liansheng Liu,[†] Stefan Kaskel,[*,§] and Yufang Zhu[*,†,‡]

[†]Hubei Key Laboratory of Processing and Application of Catalytic Materials, College of Chemical Engineering, Huanggang Normal University, Huanggang 438000, China

[‡]School of Materials Science and Engineering, University of Shanghai for Science and Technology, 516 Jungong Road, Shanghai 200093, China

[§]Professur für Anorganische Chemie I, Fachrichtung Chemie und Lebensmittelchemie, Technische Universität Dresden, Bergstrasse 66, Dresden 01062, Germany

Supporting Information

ABSTRACT: In this study, a simple one-pot method was used to prepare a multifunctional platform for synergistic chemo- and photothermal therapy,, which is composed of zeolitic imidazolate framework-8 (ZIF-8) as drug nanocarriers and the embedded graphene quantum dots (GQDs) as local photothermal seeds. The structure, drug release behavior, photothermal effect, and synergistic therapeutic efficiency of the ZIF-8/GQD nanoparticles were systematically investigated. Using doxorubicin (DOX) as a model anticancer drug, the results showed that monodisperse ZIF-8/GQD nanoparticles with a particle size of 50−100 nm could encapsulate DOX during the synthesis procedure and trigger DOX release under acidic conditions. The DOX-loaded ZIF-8/GQD nanoparticles could efficiently convert near-infrared (NIR) irradiation into heat and thereby increase the temperature. More importantly, with breast cancer 4T1 cells as a model cellular system, the results indicated that the combined chemo- and photothermal therapy with DOX-ZIF-8/GQD nanoparticles exhibited a significant synergistic effect, resulting in a higher efficacy to kill cancer cells compared with chemotherapy and photothermal therapy alone. Hence, ZIF-8/GQD nanoparticles would be promising as versatile nanocarriers for synergistic cancer therapy.

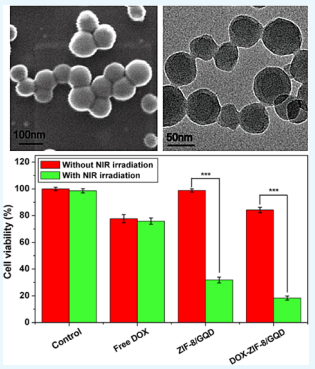

INTRODUCTION

Chemotherapy with toxic chemotherapeutic drugs is a common therapeutic approach in cancer therapy. However, direct injection of chemotherapeutic drugs has a low therapeutic efficiency and causes undesirable side effects on normal cells.[1] To date, much effort has been made to design carriers for enhancing the delivery efficiency and reducing the side effects of toxic drugs.[2] Liposomes, polymers, and dendrimers are often used as organic carriers for drug delivery owing to their high biocompatibility and biodegradability; but, their stability is low, and controlled drug release is a challenge.[3−6] By contrast, inorganic carriers such as gold and mesoporous silica have a high chemical/physiological stability and multifunctionality, but their biocompatibility and biodegradability are under debate.[7−10] Metal−organic frameworks (MOFs) are built from metal ions and organic linkers and have porous crystalline networks with a high pore volume and surface area, biodegradability, and versatile functionalities, which show a promising potential in biomedical applications such as drug delivery and/or imaging.[11,12]

Zeolitic imidazolate framework-8 (ZIF-8) is a type of nontoxic biocompatible MOF, consisting of inorganic zinc ions acting as nodes connected by 2-methylimidazolate linkers.[13] Furthermore, ZIF-8 is stable under physiological conditions and decomposes under acidic conditions, resulting in the possibility to construct pH-sensitive drug−delivery systems.[14] Drug loading in ZIF-8 is often used for postsynthesis approaches.[15−17] For example, Sun et al. loaded 5-Fu in ZIF-8 nanoparticles after ZIF-8 synthesis, and the release results showed that approximately 50% of 5-Fu was released via slow release during the early stage in a pH 7.4 solution, but the 5-Fu release rate was significantly increased in a pH 5 solution.[15] However, the postsynthesis approaches are only suitable for loading small molecular drugs because of the small diameter of the pore outlets of MOF and often result in low drug loadings and rapid or poorly controlled release of drug molecules. Recently, studies have demonstrated a "ship-in-a-bottle" strategy to encapsulate drug molecules during the synthesis of MOFs, which overcomes the drawbacks of postsynthesis approaches to some extent.[18−20] For example, Liédana et al. achieved in situ encapsulation of caffeine in ZIF-8 nanoparticles with a high loading capacity of 28 wt % and a controlled release

Received: November 11, 2016
Accepted: February 17, 2017
Published: March 31, 2017

DOI: 10.1021/acsomega.6b00385
ACS Omega 2017, 2, 1249−1258

over 27 days.[18] Zheng et al. reported one-pot synthesis of ZIF-8 with encapsulated doxorubicin (DOX) molecules, which showed promise in pH-responsive drug delivery.[20]

However, controlled drug delivery is not enough to treat cancers because of the multidrug resistance of cancer cells.[21] Currently, many studies are proposing the combination of chemotherapy with other therapeutic approaches, such as magnetic hyperthermia, photothermal therapy, and gene therapy, to obtain synergistic therapeutic effects.[22−24] Among them, photothermal therapy is a minimally invasive local treatment that uses the photoabsorbers located in tumors to convert near-infrared (NIR) energy into heat, resulting in irreversible cellular damage and subsequent tumor destruction.[25] Therefore, functionalization of ZIF-8 with photoabsorbers could form a multifunctional platform for the combination of controlled drug delivery and photothermal therapy and thereby enhance the therapeutic efficiency.

To date, a variety of photoabsorbers including gold nanorods, copper chalcogenides, and carbon nanomaterials have been investigated for photothermal therapy.[26−28] Graphene oxide (GO) including sheets and graphene quantum dots (GQDs) has gained growing attention as a photoabsorber because of its good NIR absorbance, high photothermal conversion efficiency, excellent thermal conductivity, and low toxicity.[29−31] Furthermore, the hydroxyl, epoxy, and carboxyl groups on GO enable to functionalize the MOF for the formation of MOF/GO composite nanoparticles, which could endow the MOF nanoparticles with the photothermal effect. On the one hand, studies demonstrated that MOF nanoparticles could be easily functionalized with various materials.[32−36] For example, Wuttke et al. reported the synthesis of MOF/lipid nanoparticles as nanocarriers for controlled drug delivery or imaging.[32] Wang et al. designed a targeting drug−delivery system based on bicyclononyne functionalized β-cyclodextrin derivative (β-CD-SS-BCN) functionalized MIL-101 nanoparticles, which exhibited a controlled drug release because of the pH-responsive benzoic imine bond and the redox-responsive disulfide bond on the modified surface.[33] On the other hand, many studies have recently reported MOF/graphene composite materials in different applications.[37−44] For example, Biswal et al. proposed a simple strategy to encapsulate and stabilize GO inside of ZIF-8 nanoparticles, which results in tailing the photoluminescent emission of GO@ZIF-8 nanocrystals even after 3 months of aging.[37] Zhou et al. synthesized a reduced GO (rGO)@MIL-101 composite using a solvothermal method, and the rGO@MIL-101 nanoparticles exhibited a high adsorption capacity for acetone.[38] Huang and Liu prepared a rGO/NH_2-MIL-125(Ti) hybrid nanocomposite photocatalyst and found that the composite exhibited a more efficient photocatalytic performance than NH_2-MIL-125(Ti) for methyl blue degradation under visible light irradiation.[39] However, there are no reports describing the construction of MOF/GO or MOF/GQD composite nanoparticles for synergistic drug delivery and photothermal therapy.

In this study, we have developed ZIF-8/GQD multifunctional nanoparticles with encapsulation of drug molecules using a one-pot synthesis method, which could achieve synergistic-controlled drug delivery and photothermal therapy. As shown in the schematic illustration (Figure 1), using anticancer drug DOX as a model drug, DOX molecules could be in situ encapsulated into the micropores of ZIF-8 framework during crystal growth because of the formation of weak coordination bonds between DOX molecules and zinc ions.[18−20] The GQD

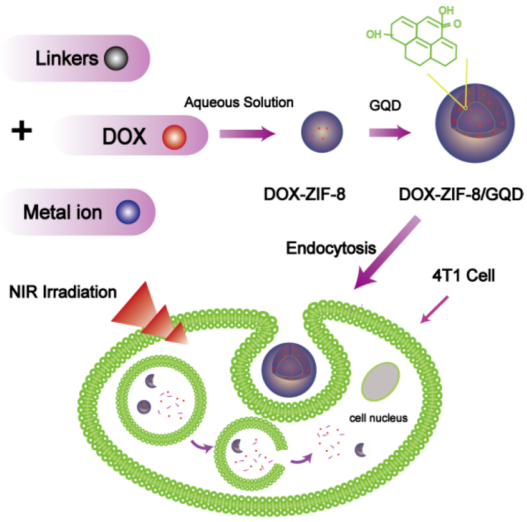

Figure 1. Schematic illustration of the synthesis of ZIF-8/GQD nanoparticles with encapsulation of DOX molecules and synergistic DOX delivery and photothermal therapy.

addition induces the adsorption of GQDs on the DOX-loaded ZIF-8 nanoparticles to form DOX-ZIF-8/GQD nanoparticles through the hydrogen bonding interaction between the N−H groups of 2-methylimidazole in ZIF-8 and the hydroxyl, epoxy, and carboxyl groups on GQDs. After endocytosis by cancer cells, the DOX-ZIF-8/GQD nanoparticles could not only realize intracellular drug release because of the acidic environment in cancer cells but also induce photothermal therapy by NIR irradiation because of the photothermal effect of GQDs.

RESULTS AND DISCUSSION

Synthesis of DOX-ZIF-8/GQD Nanoparticles. The representative scanning electron microscopy (SEM) and transmission electron microscopy (TEM) images of ZIF-8, ZIF-8/GQD, and DOX-ZIF-8/GQD nanoparticles are shown in Figure 2. It can be seen that ZIF-8/GQD and DOX-ZIF-8/GQD nanoparticles are spherical and highly monodisperse, and the particle sizes are between 50 and 100 nm. Compared with the ZIF-8 nanoparticles without GQD addition, the DOX loading and GQD addition did not significantly change the morphology of ZIF-8 nanoparticles. The particle size distributions of ZIF-8, ZIF-8/GQD, and DOX-ZIF-8/GQD nanoparticles in H_2O, phosphate-buffered saline (PBS), and Dulbecco's modified Eagle's medium (DMEM) measured using dynamic laser scattering (DLS) were relatively narrow, and the average particle sizes in different solutions were close to each other (Supporting Information), suggesting the good dispersity of ZIF-8, ZIF-8/GQD, and DOX-ZIF-8/GQD nanoparticles in aqueous solution. The average particle sizes of ZIF-8, ZIF-8/GQD, and DOX-ZIF-8/GQD nanoparticles measured using DLS were a little bigger than those observed using SEM, which might be attributed to a solvation layer around the nanoparticles for DLS measurements. When the suspensions of ZIF-8, ZIF-8/GQD, and DOX-ZIF-8/GQD nanoparticles were statically placed for 12 h, each type of suspension still exhibited good dispersity, and only a small amount of sediments was observed on the bottom (Supporting Information). It indicates that ZIF-8, ZIF-8/GQD, and DOX-ZIF-8/GQD nanoparticles could stably disperse in a physiological environment for a period of time and are beneficial for drug delivery. TEM images

DOI: 10.1021/acsomega.6b00385
ACS Omega 2017, 2, 1249−1258

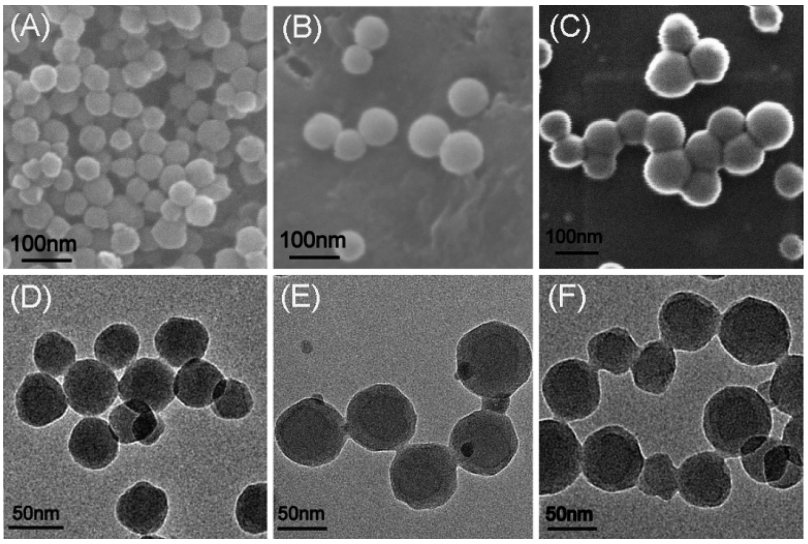

Figure 2. SEM and TEM images of ZIF-8 (A,D), ZIF-8/GQD (B,E), and DOX-ZIF-8/GQD (C,F) nanoparticles.

showed that the GQD components in the ZIF-8/GQD and DOX-ZIF-8/GQD nanoparticles were distributed at the edges of spherical ZIF-8 nanoparticles in a circular manner, which are similar to the results reported by Biswal et al.[37] In the synthesis procedure, the GQD solution was added after ZIF-8 growth for 15 min, which resulted in the GQD adsorption on the initial ZIF-8 colloidal nanoparticles because of the hydrogen bonding interaction between the N−H groups of 2-methylimidazole in ZIF-8 and the hydroxyl, epoxy, and carboxyl groups on GQDs. After GQD adsorption, the ZIF-8 nanoparticles would continue to grow owing to the residual Zn^{2+} and 2-methylimidazole in the reaction system.

The powder X-ray diffraction (XRD) patterns of ZIF-8/GQD and DOX-ZIF-8/GQD nanoparticles are shown in Figure 3. For comparison, the XRD patterns of GQDs, DOX,

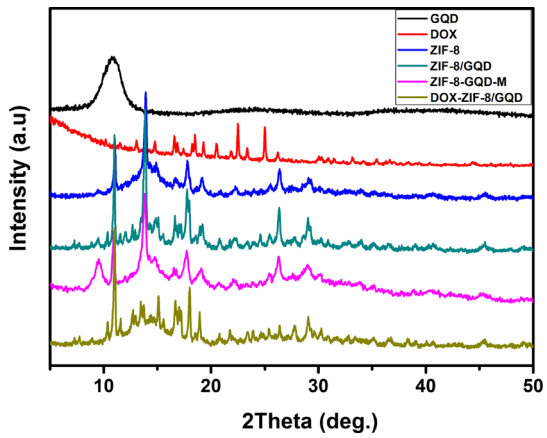

Figure 3. Wide-angle XRD patterns of GQDs, DOX, ZIF-8, ZIF-8/GQD, ZIF-8-GQDs-M, and DOX-ZIF-8/GQD nanoparticles.

and a mechanically mixed ZIF-8 and GQD sample (ZIF-8/GQDs-M) are also presented in Figure 3. ZIF-8, ZIF-8/GQD, and DOX-ZIF-8/GQD nanoparticles were highly crystalline with sharp diffraction peaks, and the ZIF-8/GQD and DOX-ZIF-8/GQD nanoparticles exhibited only peaks from ZIF-8 without any new peaks or peaks from GQDs and DOX, which is in agreement with the results of previous reports on ZIF-8/GQD composites.[40] This indicates that GQDs might form interactions with ZIF-8 in the ZIF-8/GQD and DOX-ZIF-8/GQD nanoparticles during the synthesis procedure because of the rich hydroxyl, carboxyl, and epoxy groups on GQDs and abundant N−H functional groups of 2-methylimidazole. However, the characteristic peaks of GQDs and ZIF-8 can be clearly observed in the pattern of the mechanically mixed ZIF-8/GQDs-M sample, suggesting there is no interaction between GQDs and ZIF-8 in the mechanical mixed sample. On the other hand, no peaks from DOX were observed in the pattern of DOX-ZIF-8/GQD nanoparticles, which might be attributed to the formation of amorphous DOX in the ZIF-8/GQD nanoparticles. Previous study demonstrated that DOX molecules were encapsulated in the microporous framework of ZIF-8 nanoparticles during the one-pot synthesis,[19] and the microporous framework confined the growth of the DOX crystals.

Fourier transform infrared (FTIR) spectra also confirmed the interaction between GQDs and ZIF-8 in the ZIF-8/GQD and DOX-ZIF-8/GQD nanoparticles. As shown in Figure 4, the ZIF-8/GQD and DOX-ZIF-8/GQD nanoparticles exhibit FTIR spectra similar to ZIF-8 nanoparticles. Most of the absorption bands for ZIF-8, ZIF-8/GQD, and DOX-ZIF-8/GQD nanoparticles are associated with the vibrations of the

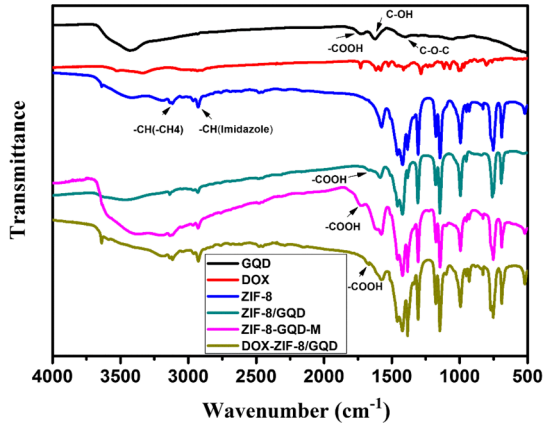

Figure 4. FTIR spectra of GQDs, DOX, ZIF-8, ZIF-8/GQD, ZIF-8-GQDs-M, and DOX-ZIF-8/GQD nanoparticles.

DOI: 10.1021/acsomega.6b00385
ACS Omega 2017, 2, 1249−1258

imidazole units, such as the peak at 1575 cm^{-1} is assigned as the C═N stretching vibration, and the bands in the range of 1350−1500 cm^{-1} are associated with the imidazole ring stretching. The strong bands at 1145 and 994 cm^{-1} are attributed to the C−N stretching of the imidazole units. However, the mechanically mixed ZIF-8 and GQD sample (ZIF-8/GQDs-M) shows not only the absorption bands from ZIF-8 but also the characteristic bands from GQDs, such as the C═O stretching vibration at 1728 cm^{-1} and the stretching deformation vibration of intercalated water at 1620 cm^{-1}. The above results indicate the interactions between ZIF-8 and GQDs in the ZIF-8/GQD and DOX-ZIF-8/GQD nanoparticles. In addition, the absorption bands for DOX in the DOX-ZIF-8/GQD nanoparticles may be overlapped with the absorption bands for ZIF-8 because of the low DOX content in the composites.

Ultraviolet−visible (UV−vis) absorption spectra could verify the DOX loading in the ZIF-8/GQD nanoparticles. As shown in Figure 5, free DOX has a characteristic absorbance peak at

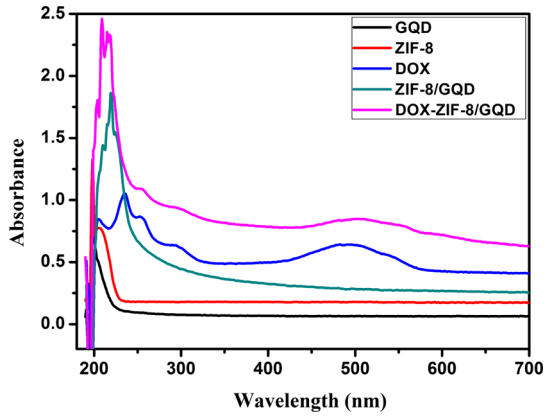

Figure 5. UV−vis spectra of the DOX solution and GQDs, ZIF-8, ZIF-8/GQD, and DOX-ZIF-8/GQD suspensions.

488 nm, which could be clearly observed on the spectrum of DOX-ZIF-8/GQD nanoparticles, whereas ZIF-8 and ZIF-8/GQDs show no peak in this region. This indicates that DOX is encapsulated in the ZIF-8/GQD nanoparticles during the synthesis procedure. By calculating the reduction in the DOX concentration from the initial DOX solution and the residual DOX amount in the supernatant after synthesis using UV−vis analysis, approximately 90% of DOX loading efficiency could be achieved, and the DOX loading capacity in the ZIF-8/GQD nanoparticles was estimated to be 47 μg/mg. As shown in the thermogravimetric (TG) analysis (Figure 6), the weight loss in the temperature range of 200−250 °C for the ZIF-8/GQD and DOX-ZIF-8/GQD nanoparticles is attributed to the decomposition of GQDs, and the weight loss for the ZIF-8/GQD and DOX-ZIF-8/GQD nanoparticles was close to each other. Notably, the DOX-ZIF-8/GQD nanoparticles showed a much higher weight loss (5.03%) than the ZIF-8/GQD nanoparticles, which is attributed to the DOX decomposition. The DOX loading amount was calculated to be 52.9 μg/mg, which is close to the result obtained using UV−vis analysis. Therefore, ZIF-8/GQD nanoparticles could encapsulate anticancer drugs to form a multifunctional platform with synergistic-controlled drug delivery and photothermal effect.

DOX Release from DOX-ZIF-8/GQD Nanoparticles. To investigate the DOX release from the DOX-ZIF-8/GQD

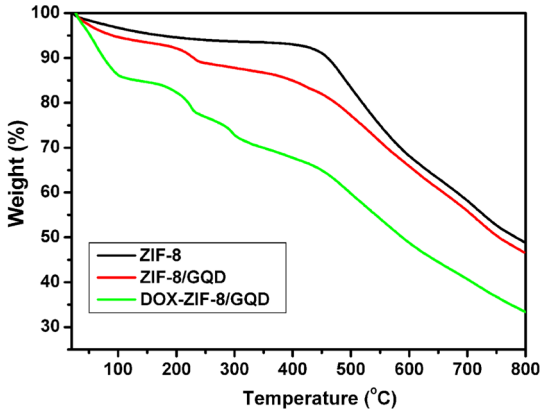

Figure 6. TG analysis of ZIF-8, ZIF-8/GQD, and DOX-ZIF-8/GQD nanoparticles.

nanoparticles under different pH conditions, the DOX-ZIF-8/GQD nanoparticles were dispersed in phosphate-buffered solution with pH 7.4, 6.0, and 4.5, separately. As shown in Figure 7, only 12% of the loaded DOX was released from the

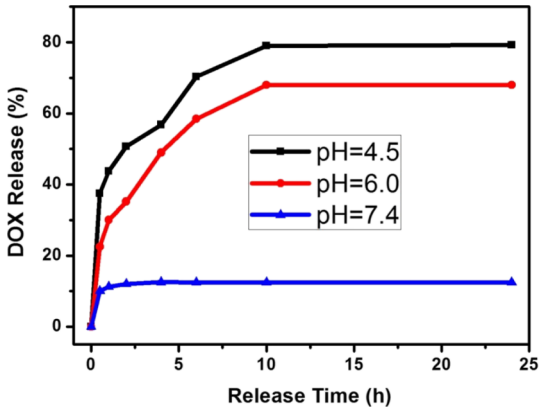

Figure 7. Cumulative DOX release profiles of DOX-ZIF-8/GQD nanoparticles in the PBS buffer with pH 4.5, 6.0, and 7.4, separately.

DOX-ZIF-8/GQD nanoparticles after 24 h in the pH 7.4 solution at 37 °C. On the contrary, DOX was released rapidly at lower pH solutions. In the pH 6.0 solution, approximately 68% of DOX was released within 24 h, and much more DOX (approximately 80%) was released in the pH 4.5 solution. Obviously, the DOX-ZIF-8/GQD nanoparticles exhibited a pH-responsive DOX release behavior. As reported before, ZIF-8 nanoparticles are stable under neutral conditions (pH 7.4) and can decompose under acidic conditions.[20] In this study, SEM was used to observe the decomposition of the DOX-ZIF-8/GQD nanoparticles in PBS at pH 7.4, 6.0, and 4.5 for different immersion times. The DOX-ZIF-8/GQD nanoparticles are spherical and have good dispersity before immersing in different PBS solutions (Figure 2). However, the morphology showed different changes after immersing in PBS at pH 7.4, 6.0, and 4.5. As shown in Figure 8, after immersing in PBS at pH 7.4 for 4 and 8 h, the DOX-ZIF-8/GQD nanoparticles still maintained a spherical morphology and good dispersity. However, when the DOX-ZIF-8/GQD nanoparticles were immersed in PBS at pH 6.0 and 4.5, the spherical nanoparticles changed to be irregular materials because of the framework decomposition. On increasing the immersing time and decreasing the pH value of PBS, more

DOI: 10.1021/acsomega.6b00385
ACS Omega 2017, 2, 1249−1258

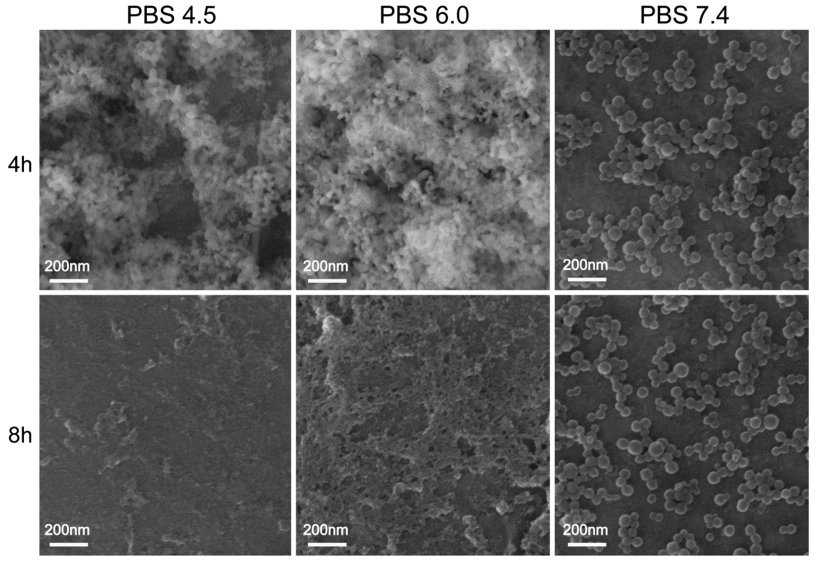

Figure 8. SEM images of DOX-ZIF-8/GQD nanoparticles after immersing in PBS with pH 4.5, 6.0, and 7.4 for 4 and 8 h.

significant morphology changes were observed, suggesting that a lower pH environment could accelerate the decomposition of the DOX-ZIF-8/GQD nanoparticles. On the other hand, the interaction between ZIF-8 and GQDs would be gradually weaker with decreasing pH value, thereby inducing the dissociation of GQDs from ZIF-8 nanoparticles. Therefore, the release of DOX from the DOX-ZIF-8/GQD nanoparticles at lower pH is associated with the dissociation of GQDs and the decomposition of ZIF-8 nanoparticles. Hence, the release behavior of the DOX-ZIF-8/GQD nanoparticles makes it interesting as a potential pH-responsive drug-delivery system for cancer therapy. In general, the physiological environment of blood stream and normal organs and tissues is neutral (pH 7.4), but it changes into an acidic condition (pH 4.5−6.0) in a tumor tissue or cancer cells.[45] Owing to the different physiological environment, the DOX molecules in the ZIF-8/GQD nanoparticles could be prevented from releasing during the delivery in blood circulation, but the DOX release could be triggered when the DOX-ZIF-8/GQD nanoparticles arrived at the tumor tissue or internalized into cancer cells. Therefore, the ZIF-8/GQD nanoparticles as nanocarriers for drug delivery could not only enhance delivery efficiency but also reduce the side effect of toxic drugs to normal organs and tissues.

Photothermal Effect of DOX-ZIF-8/GQD Nanoparticles. The DOX-ZIF-8/GQD nanoparticles had the photothermal effect because of the GQD encapsulation in the DOX-loaded ZIF-8 nanoparticles. The temperature changes under NIR irradiation at various laser intensities are shown in Figure 9A. It can be seen that the DOX-ZIF-8/GQD nanoparticles could efficiently convert NIR energy into heat and thereby increase the temperature of the DOX-ZIF-8/GQD suspension. In addition, the DOX-ZIF-8/GQD nanoparticles exhibited an excellent photothermal conversion capacity. For example, the temperature of the DOX-ZIF-8/GQD suspension at a concentration of 5 mg/mL increased from 30 °C to 49.5 °C within 10 min of irradiation at a power of 2.0 W/cm^2, and the generated heat was enough for thermal therapy. Furthermore, the temperature changes of the DOX-ZIF-8/GQD nanoparticles increased with the increase in the laser power intensity. The temperature changes of the DOX-ZIF-8/GQD suspension with different concentrations under NIR irradiation

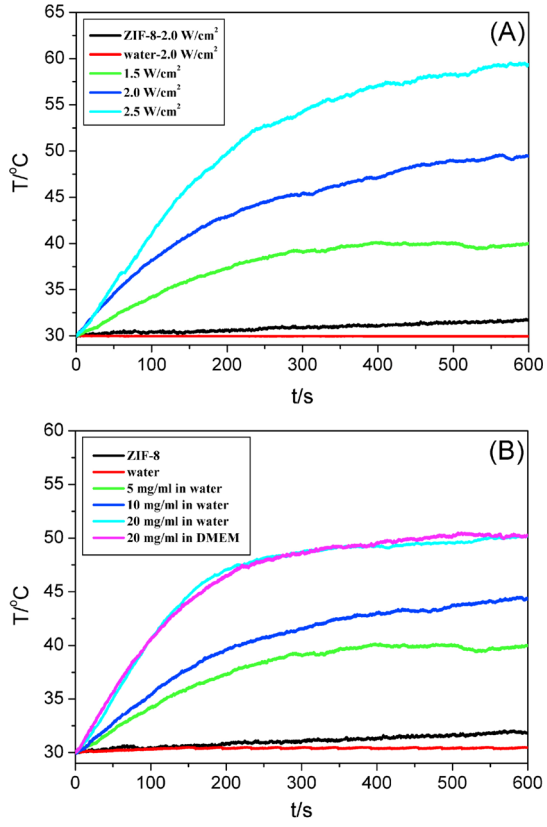

Figure 9. (A) Photothermal effects of DOX-ZIF-8/GQD nanoparticles using NIR irradiation (λ = 808 nm) at various laser intensities for 10 min; (B) Photothermal effects of DOX-ZIF-8/GQD nanoparticles in water and DMEM with different concentrations using 808 nm laser irradiation at 1.5 W/cm^2.

at 1.5 W/cm^2 are shown in Figure 9B. The photothermal effect of the DOX-ZIF-8/GQD nanoparticles enhanced with the concentration at the same laser power intensity. The temperature of the suspension at 5 mg/mL increased from 30 °C to 40 °C after 10 min of irradiation, but that at 20 mg/mL increased from 30 °C to 50.2 °C after the same irradiation time. On the other hand, the photothermal effect of the DOX-ZIF-8/GQD

DOI: 10.1021/acsomega.6b00385
ACS Omega 2017, 2, 1249−1258

nanoparticles in H_2O and culture medium DMEM at the same concentration was investigated (Figure 9B). At a concentration of 20 mg/mL, the temperature increase curve of the DOX-ZIF-8/GQD suspension in H_2O almost overlapped to that in DMEM, which suggested that the photothermal effect of the DOX-ZIF-8/GQD nanoparticles in H_2O might mimic that in the physiological environment. Therefore, the photothermal effect of the DOX-ZIF-8/GQD nanoparticles endows them with potential applications in photothermal therapy, and the therapeutic temperature can be controlled by the NIR intensity, the irradiation time, and the concentration of DOX-ZIF-8/GQD nanoparticles.

In Vitro Cytotoxicity and Cell Uptake. To evaluate the in vitro cytotoxicity of the nanocarriers and the cell uptake of the DOX-ZIF-8/GQD delivery system, breast cancer line 4T1 cells were used as a cellular system in this study. Cell viability was measured using a Cell Counting Kit-8 (CCK-8) assay to determine the in vitro cytotoxicity of the ZIF-8/GQD nanoparticles. It can be observed that the cell viabilities did not decrease even up to a concentration of 200 μg/mL, when 4T1 cells were incubated with ZIF-8/GQD nanoparticles for 24 h (Figure 10), suggesting no cytotoxicity for the ZIF-8/GQD nanoparticles. This indicates that ZIF-8/GQD nanoparticles are safe and could be used as nanocarriers for drug delivery.

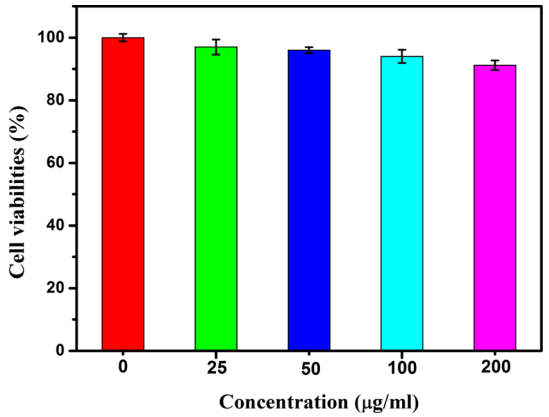

Figure 10. Cell viability of 4T1 cells after incubation with ZIF-8/GQD nanoparticles at different concentrations as measured using a CCK-8 assay.

Cell uptake of the drug delivery system is desirable in cancer therapy. For the DOX-ZIF-8/GQD nanoparticles, the internalization of the DOX-ZIF-8/GQD nanoparticles by cancer cells could not only enhance the DOX delivery efficiency but also improve the photothermal therapeutic efficacy because of the local heat generation in cancer cells. Figure 11 shows the confocal microscope images of 4T1 cells after 4 h of incubation with the free DOX, ZIF-8/GQD, and DOX-ZIF-8/GQD nanoparticles. The DOX concentration for the free DOX solution and the DOX-ZIF-8/GQD suspension was 0.5 μg/mL, and the concentration of the ZIF-8/GQD suspension was same as that of the DOX-ZIF-8/GQD suspension. For free DOX, red fluorescence from DOX was observed in 4T1 cells, suggesting that free DOX could internalize into 4T1 cells. For ZIF-8/GQD nanoparticles, green fluorescence from GQDs in 4T1 cells indicated that the ZIF-8/GQD nanoparticles internalized into 4T1 cells, whereas for the DOX-ZIF-8/GQD nanoparticles, we observed red and green fluorescence from DOX and GQDs in 4T1 cells, and the intensity of red fluorescence from DOX was a little stronger than that of free DOX, suggesting that the DOX-ZIF-8/GQD nanoparticles were easy to internalize into 4T1 cells and could release DOX efficiently in cells. On the other hand, the intensities of red fluorescence from DOX and green fluorescence from GQDs increased with the initial concentrations of the DOX-ZIF-8/GQD nanoparticles (Supporting Information), suggesting that the increase in the initial concentration could enhance the internalization capacity of the DOX-ZIF-8/GQD nanoparticles into cells. The intensities of red fluorescence from DOX and green fluorescence from GQDs also increased with incubation time (Supporting Information), which indicated that more DOX-ZIF-8/GQD nanoparticles were taken up by cells with the increase in the incubation time. Therefore, combining with the pH-responsive drug release behavior, the DOX-ZIF-8/GQD nanoparticles showed promise in intracellular drug delivery.

Synergistic Effect of Chemo- and Photothermal Therapy of DOX-ZIF-8/GQD Nanoparticles. To investigate the synergistic effect of the DOX-ZIF-8/GQD nanoparticles on therapeutic efficiency, 4T1 cells were treated for 8 h with the free DOX, ZIF-8/GQDs, and DOX-ZIF-8/GQD nanoparticles at the same concentrations and were followed by NIR irradiation for 3 min at 2.5 W/cm^2. As shown in the bright-field images (Figure 12A), without NIR irradiation, 4T1 cells treated with ZIF-8/GQD nanoparticles still showed a well-spreading cell morphology, suggesting no cell apoptosis because of the biocompatibility of the ZIF-8/GQD nanoparticles. However, the cell morphology of partial 4T1 cells changed to spherical morphology with the treatment of free DOX and DOX-ZIF-8/GQD nanoparticles, indicating apoptosis of the partial 4T1 cells, which is attributed to chemotherapy. With NIR irradiation, 4T1 cells treated with free DOX showed a similar cell morphology to that without NIR irradiation, suggesting that NIR irradiation did not influence the DOX therapeutic efficacy. However, most of 4T1 cells treated with ZIF-8/GQD and DOX-ZIF-8/GQD nanoparticles showed a spherical morphology, which indicated that NIR irradiation induced cell apoptosis significantly because of the thermal effect of ZIF-8/GQD and DOX-ZIF-8/GQD nanoparticles.

To further quantitatively evaluate the synergistic effect of the DOX-ZIF-8/GQD nanoparticles on therapeutic efficiency, cell viabilities of the treated 4T1 cells after 8 h of incubation with the free DOX, ZIF-8/GQD and DOX-ZIF-8/GQD nanoparticles were tested. As shown in Figure 12B, free DOX could kill cancer cells, and only 75% of the cell viability was obtained after the treatment by free DOX with or without NIR irradiation. Obviously, the ZIF-8/GQD nanoparticles had negligible cytotoxicity without NIR irradiation, but the cell viability decreased significantly (approximately 32%) upon NIR irradiation, which indicates the excellent photothermal therapeutic efficiency of the ZIF-8/GQD nanoparticles against cancer cells. However, it is worth noting that the cell viability decreased (approximately 84%) without NIR irradiation after incubation with the DOX-ZIF-8/GQD nanoparticles, which is attributed to the DOX release from the DOX-ZIF-8/GQD nanoparticles in cells, triggered by a lower pH environment. When NIR irradiation was applied to treat 4T1 cells after incubation with the DOX-ZIF-8/GQD nanoparticles, cell viability decreased significantly (approximately 18%), and it is also much lower than that of the ZIF-8/GQD nanoparticles with NIR irradiation. Therefore, it can be concluded that the DOX-ZIF-8/GQD nanoparticles as a multifunctional platform

DOI: 10.1021/acsomega.6b00385
ACS Omega 2017, 2, 1249−1258

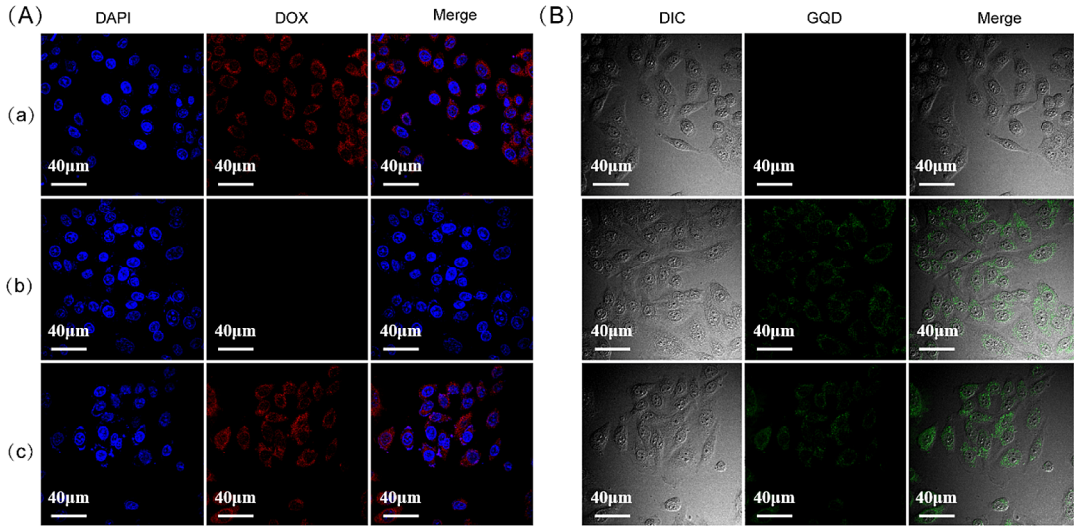

Figure 11. Confocal microscope images of 4T1 cells after 4 h of incubation with (a) free DOX, (b) ZIF-8/GQD nanoparticles, and (c) DOX-ZIF-8/GQD nanoparticles (DOX: 0.5 μg/mL, ZIF-8/GQDs: 10 μg/mL): (A) 2-(4-Amidinophenyl)-6-indolecarbamidine dihydrochloride (DAPI) and DOX channels and (B) Differential interference contrast (DIC) and GQD channels.

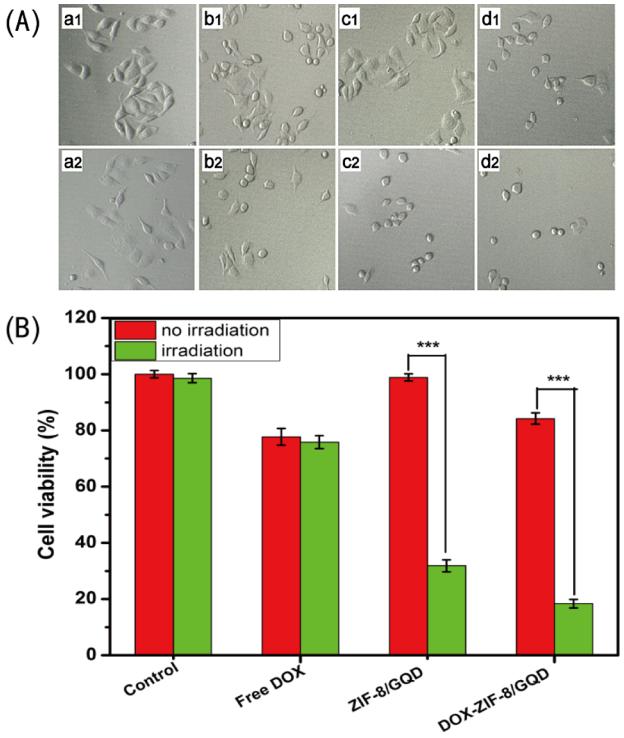

Figure 12. (A) Bright-field images of 4T1 cells after 8 h of incubation (a) without free DOX solution and (b) with free DOX solution, (c) with ZIF-8/GQD, and (d) with DOX-ZIF-8/GQD suspensions (DOX: 5 μg/mL, ZIF-8/GQDs: 100 μg/mL), the images of a1−d1 were recorded without NIR irradiation, and the images of a2−d2 were recorded after NIR irradiation for 3 min. (B) Cell viability of 4T1 cells after 8 h of incubation without and with free DOX solution, ZIF-8/GQD, and DOX-ZIF-8/GQD suspensions (DOX: 5 μg/mL, ZIF-8/GQDs: 100 μg/mL) and without and with 3 min NIR irradiation.

could achieve the synergistic therapeutic efficiency through chemo- and photothermal therapy.

EXPERIMENTAL SECTION

Materials. 2-Methylimidazole (99%), $Zn(NO_3)_2{\cdot}6H_2O$ (99%), and methanol (HPLC grade) were purchased from Sigma-Aldrich. Doxorubicin hydrochloride was purchased from Sangon Biotech (Shanghai) Co. Ltd. GQDs (1 mg/mL) were purchased from Nanjing XFNANO Co. Ltd. Ultrapure water was obtained from a Millipore pure water system. All chemicals were used without further purification.

Synthesis of ZIF-8 Nanoparticles. ZIF-8 nanoparticles were synthesized according to a previous report with some modifications.[19] Typically, 95 mg of $Zn(NO_3)_2{\cdot}6H_2O$ was dissolved in 50 mL of H_2O under magnetic agitation for 15 min. Subsequently, 200 mg (2.43 mmol) of 2-methylimidazole in 50 mL of H_2O was added to the above $Zn(NO_3)_2$ solution at room temperature, with magnetic agitation for another 1 h. Finally, the nanoparticles were collected by centrifugation and washing several times with ethanol and dried under vacuum at 60 °C for 6 h.

Synthesis of DOX-ZIF-8/GQD Nanoparticles. For a typical synthesis, 95 mg of $Zn(NO_3)_2{\cdot}6H_2O$ was dissolved in 50 mL of H_2O under magnetic agitation for 15 min, and 2 mL of DOX solution (2 mg/mL) was added to $Zn(NO_3)_2$ solution. Subsequently, 200 mg (2.43 mmol) of 2-methylimidazole in 50 mL of H_2O was added to the above solution at room temperature, with magnetic agitation for another 15 min to form a mixed suspension. Then, 1 mL of GQD solution was added to the above mixed suspension. After 1 h of reaction, the nanoparticles were collected by centrifugation and washing several times with ethanol and then dried under vacuum at 60 °C for 6 h.

As a control, the ZIF-8/GQD nanoparticles were synthesized similar to that of DOX-ZIF-8/GQD nanoparticles without the addition of DOX solution.

Characterization. SEM was carried out using an FEI Quanta 450 field emission scanning electron microscope. TEM images were obtained using a Tecnai G2 F30 electron microscope operating at an acceleration voltage of 300 kV. Powder XRD patterns were obtained using a D8 ADVANCE powder diffractometer using Cu Kα1 radiation (1.5405 Å). FTIR spectra were recorded on a LAM750(s) spectrometer in

DOI: 10.1021/acsomega.6b00385
ACS Omega 2017, 2, 1249−1258

transmission mode. TG analysis was carried out on an STA 449 F3 thermal analyzer under N_2 atmosphere with a flow rate of 20 mL/min and a heating rate of 10 °C/min. UV−vis analysis was performed using a NanoDrop 2000C spectrophotometer. Photothermal effects of the samples were measured using an infrared thermal imaging system with a diode laser.

Drug Release. To investigate the drug release behavior from the DOX-ZIF-8/GQD nanoparticles, 20 mg of DOX-ZIF-8/GQD nanoparticles was dispersed in 10 mL of PBS solution (pH 4.5, 6.0, and 7.4, separately). The release system was maintained at 37 °C under dark conditions and shaking (100 rpm). At a given time, the release system was centrifuged, and an aliquot (20 μL) of the supernatant was taken out for UV−vis analysis at the wavelength of 488 nm and replaced with the same amount of fresh medium. The release percentages of DOX were calculated according to the equation: DOX (%) = total released DOX/total loaded DOX in ZIF-8/GQDs × 100%. Before the calculation, a standard curve for the DOX solution was recorded using a NanoDrop 2000C spectrophotometer.

Photothermal Effect of DOX-ZIF-8/GQD Nanoparticles. Typically, the DOX-ZIF-8/GQD nanoparticles were dispersed in H_2O and culture medium (DMEM) at different concentrations. Subsequently, 1 mL of the DOX-ZIF-8/GQD suspension in each well of a 96-well plate was irradiated for 10 min using a diode laser (808 nm) at a distance of 1.0 cm. To determine the impacts of irradiation intensity, an 808 nm laser irradiated the DOX-ZIF-8/GQD suspensions at a concentration of 5 mg/mL, with the power intensities at 1.5, 2.0, and 2.5 W/cm^2 for 10 min. To determine the effects of the suspension concentrations, the DOX-ZIF-8/GQD suspensions at concentrations from 5 to 20 mg/mL were irradiated using an 808 nm laser at 1.5 W/cm^2 for 10 min. An infrared thermometer monitored the temperature of the DOX-ZIF-8/GQD suspensions every 30 s, and the temperature changes were transferred into a computer through the optical fiber.

Cell Culture. To evaluate the potential property of the ZIF-8/GQD and DOX-ZIF-8/GQD nanoparticles in the cellular system, breast cancer line 4T1 cells were used in this study. 4T1 cells were cultured in DMEM and supplemented with 10% fetal bovine serum, 100 units/mL penicillin, and 100 mg/mL streptomycin and incubated in 5% CO_2 atmosphere at 37 °C.

In Vitro Cytotoxicity. In vitro cytotoxicity of the ZIF-8/GQD nanoparticles was evaluated using a CCK-8 assay. Before cell culture, the ZIF-8/GQD nanoparticles sterilized with UV irradiation were dispersed in DMEM to obtain the stack solution with different concentrations. 4T1 cells were seeded in a 96-well plate at a density of 5 × 10^4 cells/well. After seeding the cells for 4 h to allow the attachment of the cells, the cells were washed with PBS, and the ZIF-8/GQD solution was immediately added into each well to achieve the final ZIF-8/GQD concentrations of 0, 25, 50, 100, and 200 μg/mL, and the final medium volume in each well was 100 μL. After incubation of cells for 24 h, 10 μL of CCK-8 solution was added into each well, and the cells were incubated for another 2 h. The absorbance at 450 nm was then measured using a microplate reader (ELX800, BioTek). Cytotoxicity was expressed as the percentage of viable cells compared with that of untreated control cells.

Cell Uptake. To verify the cell uptake of the DOX-ZIF-8/GQD nanoparticles, 4T1 cells were seeded in a 35 mm Petri dish with 1 × 10^5 cells and cultured for 12 h to attach on the bottom. After the cells were washed with PBS, 0.5 mL of DOX-ZIF-8/GQD solution in DMEM was added into the Petri dish with a concentration from 5 to 15 μg/mL. Free DOX and ZIF-8/GQD nanoparticles were used for comparison. After incubation of cells for 2, 4, and 8 h, the cells were washed with PBS three times to remove the extracellular nanoparticles and dead cells. Then, 1.5 mL of DAPI methanolic solution was added to the Petri dish to stain the nuclei of 4T1 cells for 15 min. Finally, the cells were washed several times with PBS and were observed using a confocal laser scanning microscope (CLSM, Leica, SP8).

Synergistic Chemo- and Photothermal Therapy of DOX-ZIF-8/GQD Nanoparticles on Cancer Cells. 4T1 cells were seeded into a 96-well plate at a density of 1 × 10^5 cells/well and incubated for 4 h to allow the attachment of the cells. After the removal of the culture medium, 100 μL of DOX-ZIF-8/GQD solution (100 μg/mL in DMEM, [DOX] = 5 μg/mL) was added into each well. The same concentrations of free DOX solution (5 μg/mL) and ZIF-8/GQD solution (100 μg/mL) were used for comparison. After incubation of cells for 8 h, the cells were washed with PBS and fresh DMEM was added. Then, the cells were irradiated for 3 min using an 808 nm laser at a distance of 1.0 cm and a power intensity of 2.5 w/cm^2. After irradiation, the cells were cultured for 4 h and then observed using fluorescence microscopy. After that, 10 μL of CCK-8 solution was added into each well, and the cells were incubated for another 2 h. The absorbance at 450 nm was measured using a microplate reader (ELX800, BioTek). Cell viability was expressed in comparison with that of untreated control cells.

CONCLUSIONS

In this study, we reported the synthesis of ZIF-8/GQD multifunctional nanoparticles with encapsulation of anticancer drug for synergistic chemo- and photothermal therapy. The DOX-ZIF-8/GQD nanoparticles were monodisperse, and the particle size was approximately 50−100 nm. They could not only generate heat efficiently to increase the temperature because of NIR irradiation but also have a pH-responsive drug release behavior. Using breast cancer 4T1 cells as a cellular system, the ZIF-8/GQD nanoparticles had negligible cytotoxicity and the DOX-ZIF-8/GQD nanoparticles could be taken up by 4T1 cells. Interestingly, the DOX-ZIF-8/GQD nanoparticles showed a synergistic effect to kill cancer cells because of the pH-controlled DOX release and the photothermal effect of GQDs. Therefore, the DOX-ZIF-8/GQD nanoparticles would be a promising multifunctional system for potential cancer therapy.

ASSOCIATED CONTENT

Supporting Information

The Supporting Information is available free of charge on the ACS Publications website at DOI: 10.1021/acsomega.6b00385.

Particle sizes measured using DLS and stabilities of the ZIF-8, ZIF-8/GQD, and DOX-ZIF-8/GQD nanoparticles in water, PBS, and culture medium; and cell uptake of the DOX-ZIF-8/GQD nanoparticles at different concentrations and incubation times (PDF)

AUTHOR INFORMATION

Corresponding Authors

*E-mail: stefan.kaskel@chemie.tu-dresden.de (S.K.).
*E-mail: zjf2412@163.com (Y.Z.).

DOI: 10.1021/acsomega.6b00385
ACS Omega 2017, 2, 1249−1258

Author Contributions

[‖]Z.T. and X.Y. contributed equally to this work.

Notes

The authors declare no competing financial interest.

■ ACKNOWLEDGMENTS

The authors gratefully acknowledge the support by the National Natural Science Foundation of China (no. 51572172, 51102166) and the Alexander von Humboldt Foundation.

■ REFERENCES

(1) Cho, K.; Wang, X.; Nie, S.; Chen, Z.; Shin, D. M. Therapeutic nanoparticles for drug delivery in cancer. *Clin. Cancer Res.* **2008**, *14*, 1310−1316.

(2) Petros, R. A.; DeSimone, J. M. Strategies in the design of nanoparticles for therapeutic applications. *Nat. Rev. Drug Discovery* **2010**, *9*, 615−627.

(3) Li, W.-Z.; Hao, X.-L.; Zhao, N.; Han, W.-X.; Zhai, X.-F.; Zhao, Q.; Wang, Y.-E.; Zhou, Y.-Q.; Cheng, Y.-C.; Yue, Y.-H.; Fu, L.-N.; Zhou, J.-L.; Wu, H.-Y.; Dong, C.-J. Propylene glycol-embodying deformable liposomes as a novel drug delivery carrier for vaginal fibrauretine delivery applications. *J. Controlled Release* **2016**, *226*, 107−114.

(4) Hu, X.; Zhang, Y.; Zhou, H.; Wan, H. PEGylated chitosan microspheres as mucoadhesive drug-delivery carriers for puerarin. *J. Appl. Polym. Sci.* **2015**, *132*, 42623.

(5) Zhang, Z.; Tang, J.; Liu, X.; Shen, Y. Synthesis and characterization of phosphate structured dendrimers as drug delivery carriers. *Nanomedicine: Nanotechnology, Biology and Medicine* **2016**, *12*, 473.

(6) Eckmann, D. M.; Composto, R. J.; Tsourkas, A.; Muzykantov, V. R. Nanogel carrier design for targeted drug delivery. *J. Mater. Chem. B* **2014**, *2*, 8085−8097.

(7) Khandelia, R.; Bhandari, S.; Pan, U. N.; Ghosh, S. S.; Chattopadhyay, A. Gold Nanocluster Embedded Albumin Nanoparticles for Two-Photon Imaging of Cancer Cells Accompanying Drug Delivery. *Small* **2015**, *11*, 4075−4081.

(8) Majeed, M. I.; Lu, Q.; Yan, W.; Li, Z.; Hussain, I.; Tahir, M. N.; Tremel, W.; Tan, B. Highly water-soluble magnetic iron oxide (Fe_3O_4) nanoparticles for drug delivery: Enhanced in vitro therapeutic efficacy of doxorubicin and MION conjugates. *J. Mater. Chem. B* **2013**, *1*, 2874−2884.

(9) Karimi, M.; Mirshekari, H.; Aliakbari, M.; Sahandi-Zangabad, P.; Hamblin, M. R. Smart mesoporous silica nanoparticles for controlled-release drug delivery. *Nanotechnol. Rev.* **2016**, *5*, 195−207.

(10) Chen, S.; Hao, X.; Liang, X.; Zhang, Q.; Zhang, C.; Zhou, G.; Shen, S.; Jia, G.; Zhang, J. Inorganic Nanomaterials as Carriers for Drug Delivery. *J. Biomed. Nanotechnol.* **2016**, *12*, 1−27.

(11) Horcajada, P.; Chalati, T.; Serre, C.; Gillet, B.; Sebrie, C.; Baati, T.; Eubank, J. F.; Heurtaux, D.; Clayette, P.; Kreuz, C.; Chang, J.-S.; Hwang, Y. K.; Marsaud, V.; Bories, P.-N.; Cynober, L.; Gil, S.; Férey, G.; Couvreur, P.; Gref, R. Porous metal−organic-framework nanoscale carriers as a potential platform for drug delivery and imaging. *Nat. Mater.* **2009**, *9*, 172−178.

(12) Cai, W.; Chu, C.-C.; Liu, G.; Wáng, Y.-X. J. Metal−Organic Framework-Based Nanomedicine Platforms for Drug Delivery and Molecular Imaging. *Small* **2015**, *11*, 4806−4822.

(13) Broadley, M. R.; White, P. J.; Hammond, J. P.; Zelko, I.; Lux, A. Zinc in plants. *New Phytol.* **2007**, *173*, 677−702.

(14) Adhikari, C.; Das, A.; Chakraborty, A. Zeolitic Imidazole Framework (ZIF) Nanospheres for Easy Encapsulation and Controlled Release of an Anticancer Drug Doxorubicin under Different External Stimuli: A Way toward Smart Drug Delivery System. *Mol. Pharm.* **2015**, *12*, 3158−3166.

(15) Sun, C.-Y.; Qin, C.; Wang, X.-L.; Yang, G.-S.; Shao, K.-Z.; Lan, Y.-Q.; Su, Z.-M.; Huang, P.; Wang, C.-G.; Wang, E.-B. Zeolitic imidazolate framework-8 as efficient pH-sensitive drug delivery vehicle. *Dalton Trans.* **2012**, *41*, 6906−6909.

(16) Lyu, F.; Zhang, Y.; Zare, R. N.; Ge, J.; Liu, Z. One-pot synthesis of protein-embedded metal−organic frameworks with enhanced biological activities. *Nano Lett.* **2014**, *14*, 5761−5765.

(17) Vasconcelos, I. B.; da Silva, T. G.; Militão, G. C. G.; Soares, T. A.; Rodrigues, N. M.; Rodrigues, M. O.; Da Costa, N. B., Jr.; Freire, R. O.; Junior, S. A. Cytotoxicity and slow release of the anti-cancer drug doxorubicin from ZIF-8. *RSC Adv.* **2012**, *2*, 9437−9442.

(18) Liédana, N.; Galve, A.; Rubio, C.; Téllez, C.; Coronas, J. CAF@ZIF-8: One-Step Encapsulation of Caffeine in MOF. *ACS Appl. Mater. Interfaces* **2012**, *4*, 5016−5021.

(19) Zhuang, J.; Kuo, C.-H.; Chou, L.-Y.; Liu, D.-Y.; Weerapana, E.; Tsung, C.-K. Optimized Metal−Organic-Framework Nanospheres for Drug Delivery: Evaluation of Small-Molecule Encapsulation. *ACS Nano* **2014**, *8*, 2812−2819.

(20) Zheng, H.; Zhang, Y.; Liu, L.; Wan, W.; Guo, P.; Nyström, A. M.; Zou, X. One-pot synthesis of metal-organic frameworks with encapsulated target-molecules and their applications for controlled drug delivery. *J. Am. Chem. Soc.* **2016**, *138*, 962−968.

(21) Jelovac, D.; Armstrong, D. K. Recent progress in the diagnosis and treatment of ovarian cancer. *Ca-Cancer J. Clin.* **2011**, *61*, 183−203.

(22) Sasikala, A. R. K.; Thomas, R. G.; Unnithan, A. R.; Saravanakumar, B.; Jeong, Y. Y.; Park, C. H.; Kim, C. S. Multifunctional Nanocarpets for Cancer Theranostics: Remotely Controlled Graphene Nanoheaters for Thermo-Chemosensitisation and Magnetic Resonance Imaging. *Sci. Rep.* **2016**, *6*, 20543.

(23) Liu, J.; Detrembleur, C.; De Pauw-Gillet, M.-C.; Mornet, S.; Jérôme, C.; Duguet, E. Gold nanorods coated with mesoporous silica shell as drug delivery system for remote near infrared light-activated release and potential phototherapy. *Small* **2015**, *11*, 2323−2332.

(24) Xu, Q.; Leong, J.; Chua, Q. Y.; Chi, Y. T.; Chow, P. K.-H.; Pack, D. W.; Wang, C.-H. Combined modality doxorubicin-based chemotherapy and chitosan-mediated p53 gene therapy using double-walled microspheres for treatment of human hepatocellular carcinoma. *Biomaterials* **2013**, *34*, 5149−5162.

(25) Shen, S.; Wang, S.; Zheng, R.; Zhu, X.; Jiang, X.; Fu, D.; Yang, W. Magnetic nanoparticle clusters for photothermal therapy with near-infrared irradiation. *Biomaterials* **2015**, *39*, 67−74.

(26) Li, C.; Chen, T.; Ocsoy, I.; Zhu, G.; Yasun, E.; You, M.; Wu, C.; Zheng, J.; Song, E.; Huang, C. Z.; Tan, W. Gold-Coated Fe_3O_4 Nanoroses with Five Unique Functions for Cancer Cell Targeting, Imaging, and Therapy. *Adv. Funct. Mater.* **2014**, *24*, 1772−1780.

(27) Bai, J.; Liu, Y.; Jiang, X. Multifunctional PEG−GO/CuS nanocomposites for near-infrared chemo-photothermal therapy. *Biomaterials* **2014**, *35*, 5805−5813.

(28) Acik, M.; Lee, G.; Mattevi, C.; Chhowalla, M.; Cho, K.; Chabal, Y. J. Unusual infrared-absorption mechanism in thermally reduced graphene oxide. *Nat. Mater.* **2010**, *9*, 840−845.

(29) Biswal, B. P.; Shinde, D. B.; Pillai, V. K.; Banerjee, R. Stabilization of graphene quantum dots (GQDs) by encapsulation inside zeolitic imidazolate framework nanocrystals for photoluminescence tuning. *Nanoscale* **2013**, *5*, 10556−10561.

(30) Wang, Y.; Wang, K.; Zhao, J.; Liu, X.; Bu, J.; Yan, X.; Huang, R. Multifunctional Mesoporous Silica-Coated Graphene Nanosheet Used for Chemo-Photothermal Synergistic Targeted Therapy of Glioma. *J. Am. Chem. Soc.* **2013**, *135*, 4799−4804.

(31) Yang, K.; Feng, L.; Liu, Z. The advancing uses of nano-graphene in drug delivery. *Expert Opin. Drug Delivery* **2015**, *12*, 601−612.

(32) Wuttke, S.; Braig, S.; Preiß, T.; Zimpel, A.; Sicklinger, J.; Bellomo, C.; Rädler, J. O.; Vollmar, A. M.; Bein, T. MOF nanoparticles coated by lipid bilayers and their uptake by cancer cells. *Chem. Commun.* **2015**, *51*, 15752−15755.

(33) Wang, X.-G.; Dong, Z.-Y.; Cheng, H.; Wan, S.-S.; Chen, W.-H.; Zou, M.-Z.; Huo, J.-W.; Deng, H.-X.; Zhang, X.-Z. A multifunctional metal−organic framework based tumor targeting drug delivery system for cancer therapy. *Nanoscale* **2015**, *7*, 16061−16070.

(34) Ren, H.; Zhang, L.; An, J.; Wang, T.; Li, L.; Si, X.; He, L.; Wu, X.; Wang, C.; Su, Z. Polyacrylic acid@zeolitic imidazolate framework-8

DOI: 10.1021/acsomega.6b00385
ACS Omega 2017, 2, 1249−1258

nanoparticles with ultrahigh drug loading capability for pH-sensitive drug release. *Chem. Commun.* **2014**, *50*, 1000−1002.
(35) Deng, K.; Hou, Z.; Li, X.; Li, C.; Zhang, Y.; Deng, X.; Cheng, Z.; Lin, J. Aptamer-Mediated Up-Conversion Core/MOF Shell Nanocomposites for Targeted Drug Delivery and Cell Imaging. *Sci. Rep.* **2015**, *5*, 7851.
(36) Ke, F.; Yuan, Y.-P.; Qiu, L.-G.; Shen, Y.-H.; Xie, A.-J.; Zhu, J.-F.; Tian, X.-Y.; Zhang, L.-D. Facile fabrication of magnetic metal−organic framework nanocomposites for potential targeted drug delivery. *J. Mater. Chem.* **2011**, *21*, 3843−3848.
(37) Biswal, B. P.; Shinde, D. B.; Pillai, V. K.; Banerjee, R. Stabilization of graphene quantum dots (GQDs) by encapsulation inside zeolitic imidazolate framework nanocrystals for photoluminescence tuning. *Nanoscale* **2013**, *5*, 10556−10561.
(38) Zhou, X.; Huang, W.; Shi, J.; Zhao, Z.; Xia, Q.; Li, Y.; Wang, H.; Li, Z. A novel MOF/graphene oxide composite GrO@MIL-101 with high adsorption capacity for acetone. *J. Mater. Chem. A* **2014**, *2*, 4722−4730.
(39) Huang, L.; Liu, B. Synthesis of a novel and stable reduced graphene oxide/MOF hybrid nanocomposite and photocatalytic performance for the degradation of dyes. *RSC Adv.* **2016**, *6*, 17873−17879.
(40) Chen, B.; Zhu, Y.; Xia, Y. Controlled in situ synthesis of graphene oxide/zeolitic imidazolate framework composites with enhanced CO_2 uptake capacity. *RSC Adv.* **2015**, *5*, 30464−30471.
(41) Yang, L.; Tang, B.; Wu, P. Metal−organic framework−graphene oxide composites: A facile method to highly improve the proton conductivity of PEMs operated under low humidity. *J. Mater. Chem. A* **2015**, *3*, 15838−15842.
(42) Zhao, M.; Zhang, X.; Deng, C. Facile synthesis of hydrophilic magnetic graphene@metal−organic framework for highly selective enrichment of phosphopeptides. *RSC Adv.* **2015**, *5*, 35361−35364.
(43) Hu, Y.; Wei, J.; Liang, Y.; Zhang, H.; Zhang, X.; Shen, W.; Wang, H. Zeolitic Imidazolate Framework/Graphene Oxide Hybrid Nanosheets as Seeds for the Growth of Ultrathin Molecular Sieving Membranes. *Angew. Chem., Int. Ed.* **2016**, *55*, 2048−2052.
(44) Tian, Z.; Yao, X.; Zhu, Y. Simple synthesis of multifunctional zeolitic imidazolate frameworks-8/graphene oxide nanocrystals with controlled drug release and photothermal effect. *Microporous Mesoporous Mater.* **2017**, *237*, 160−167.
(45) Tao, C.; Zhu, Y. Magnetic mesoporous silica nanoparticles for potential delivery of chemotherapeutic drugs and hyperthermia. *Dalton Trans.* **2014**, *43*, 15482−15490.

DOI: 10.1021/acsomega.6b00385
ACS Omega 2017, 2, 1249−1258